Published Journal Article available at: http://dx.doi.org/10.1016/j.enconman.2017.03.010

Process modeling of a reversible solid oxide cell (r-SOC) energy storage system utilizing commercially available SOC reactor

Pegah Mottaghizadeh [a, b], Srikanth Santhanam [a, *], Marc P. Heddrich [a], K. Andreas Friedrich [a], Fabio Rinaldi [b]

[a] German Aerospace Center (DLR), Institute of Engineering Thermodynamics, Pfaffenwaldring 38-40, 70569 Stuttgart, Germany
[b] Politecnico di Milano, Piazza Leonardo da Vinci, 32, 20133 Milano, Italy

The increase of intermittent renewable energy contribution in power grids has urged us to seek means for temporal de-coupling of electricity production and consumption. A reversible solid oxide cell (r-SOC) enables storage of surplus elec-tricity through electrochemical reactions when it is in electrolysis mode. The reserved energy in form of chemical com-pounds is then converted to electricity when the cell operates as a fuel cell. A process system model was implemented using Aspen Plus® V8.8 based on a commercially available r-SOC reactor experimentally characterized at DLR. In this study a complete self-sustaining system configuration is designed by optimal thermal integration and balance of plant. Under reference conditions a round trip efficiency of 54.3% was achieved. Generated heat in fuel cell mode is exploited by latent heat storage tanks to enable endothermic operation of reactor in its electrolysis mode. In total, out of 100units of thermal energy stored in heat storage tanks during fuel cell mode, 90% was utilized to offset heat demand of system in its electrolysis mode. Parametric analysis revealed the significance of heat storage tanks in thermal management even when reactor entered its exothermic mode of electrolysis. An improved process system design demonstrates a system round-trip efficiency of 60.4% at 25 bar. .

Keywords: Reversible solid oxide cell (r-SOC), Electrical energy storage (EES), Latent heat storage, Round-trip efficiency

1. Introduction

The growing penetration of renewable energy sources (RES) to power grids entails some challenges that need to be tackled. The intermittent and unpredictable nature of wind and solar power make it necessary to balance the time varying demand and supply in power network. Electrical energy storage (EES) boosts the reliability of power supply, stability of the grid, and quality of voltage [1]. Different technologies of EES such as compressed air, pumped hydroelectric, and battery have been proposed with their own pros and cons [2–7]. Conversion of electricity to chemical energy is an advantageous alternative thanks to its high energy density capacity [8,9]. Moreover, the high value chemical compounds produced by electrochemical reactions could be further utilized by the chemical industry [10,11]. The regenerative solid oxide cell (r-SOC) is a means of EES that incorporates both charging and discharging of electricity in one reactor. The concept is new and few modeling and experimental investigations have been done on r-SOC systems [12–16] or material development [17–19]. High operating temperature required for electrochemical reactions occurring inside r-SOC (750–1000 °C) results in lower electrochemical loss and hence higher performance. This characteristic of r-SOC systems makes them superior to other electrochemical reactors [20]. Electrochemical reactions could be based on either H-O or H-O-C elemental systems. In H-O-based systems, only hydrogen, water, and oxygen are involved; while in H-O-C-based systems also hydrocarbons participate in reactions and therefore extend the application range of r-SOC systems. This paper investigates H-C-O-based r-SOC system. During charging, SOC operates as electrolyzer converting electricity to chemical energy via co-electrolysis of H_2O and CO_2 generating fuel such as H_2 and carbonaceous compounds. During discharge, r-SOC operates as fuel cell generating electricity via the electrochemical oxidation of fuel [21,22]. Operating electrolysis mode of r-SOC in its endothermic mode gives rise to an enhanced cell performance and subsequently higher system round-trip efficiency [23]. The exothermic nature of oxidation reactions in fuel cell mode and endothermic behavior during electrolysis necessitates an efficient thermal management system. Utilization of heat generated due to exothermic reactions in solid oxide fuel cell (SOFC) mode is an effective recourse to compensate the heat demand for endothermic operation of solid oxide electrolysis cell (SOEC) [24]. Application of thermal energy storage (TES) in r-SOC system boosts thermal management by storing the released heat in SOFC and consuming it for SOEC operation. In this work, a cascaded latent heat storage system with appropriate phase change materials is integrated with a commercially available solid oxide cell experimentally characterized at DLR [25,26]. A downstream process like methanation is also incorporated into the system for its beneficial implications on thermal management as well as hydrocarbon production. As a consequence, a thermally self-sustaining process system is designed for this r-SOC reactor with the required balance of plant. Performance of the system is studied under reference conditions, followed by parametric analysis. Based on the results from the parametrical analysis, an improved process system model is pro-

Article history:
Received 9 January 2017
Received in revised form 2 March 2017
Accepted 3 March 2017
Available online xxx

* Corresponding author.
Email address: Srikanth.Santhanam@dlr.de (S. Santhanam)

posed and investigated for maximum performance of the available r-SOC reactor.

2. Description of process system components

Simple schematic design of r-SOC system for charging and discharging modes are provided in Figs. 1 and 2. Fig. 1 depicts the r-SOC system during charging or fuel production mode (SOEC). When the electricity supplied from intermittent sources is more than demand, it could be stored within r-SOC system by following process: H_2O and CO_2 required for electrolysis are primarily preheated in heat recovery units to cool down the outlet streams. The required heat for endothermic electrolysis is supplied through inlet process gasses by directing them to TES units. Electricity is converted to syngas (H_2, CO) as a result of electrochemical and chemical reactions inside r-SOC. The product gases undergo further chemical reactions in downstream processes such as methanation or Fischer-Tropsch depending on the requirements. Finally, the products are cooled and separated from the steam, compressed and kept in a fuel tank. Fig. 2 represents the discharging mode (SOFC), where the fuel produced from SOEC operation is utilized in the fuel cell. After being mixed with the required steam for coke prevention, process gases are preheated and reached equilibrium before entering the r-SOC. Fuel gases are oxidized to provide electricity. Considerable amount of heat is generated due to exothermic reactions and losses in the SOFC. This heat is harnessed through a TES system and the remaining heat is used for preheating the inlet streams. The exhaust gases are subsequently separated from the steam, compressed and stored in a fuel tank. Air, as an essential agent for both operations is supplied to the air channel of the r-SOC after being preheated by outlet air streams. It provides the required oxygen for oxidation and cools down the reactor during exothermic SOFC operation; whereas, for endothermic SOEC operation it acts as heating medium and sweep gas to flush the produced oxygen. Brief description of the components is provided in the following subsections.

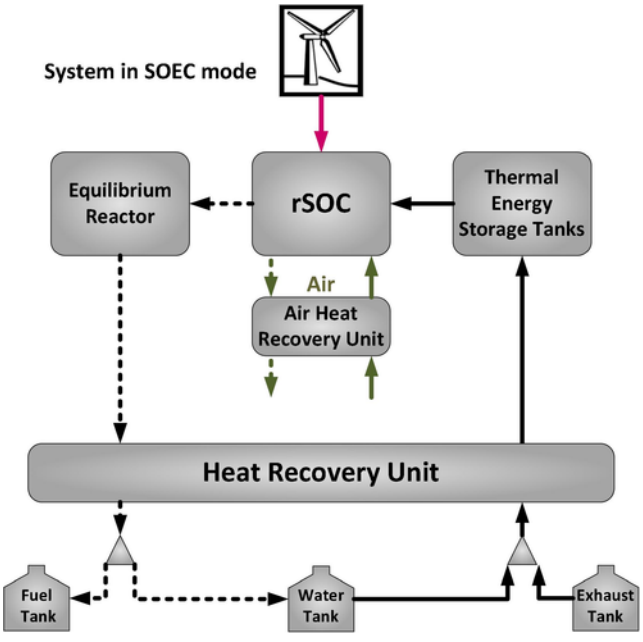

Fig. 1. Simple schematic of r-SOC system in charging mode (SOEC).

2.1. Solid oxide cell electrochemical reactor (SOC)

A solid oxide cell is an electrochemical reactor capable of direct conversion of electricity to fuel (electrolysis) and fuel to electricity (oxidation) owing to the identical infrastructures required for SOFC and SOEC. Each cell is composed of a fuel electrode, ion electrolyte and air electrode. Electrolytes are made of nonporous solid ceramics like YSZ with high ionic and low electrical conductivity [27]. The electrodes are made of porous and electrically conductive composites such as Ni-YSZ for fuel side and LSM-YSZ for air side [28]. Base on the mechanical structure, the cells are categorized as electrolyte supported cell (ESC) with high ohmic resistance due to thick electrolyte or as anode supported cell (ASC) with thin electrolyte layer and lower overpotential loss [29,30]. The operating temperature of SOC varies from intermediate to high values, 600–1000 °C enabling their integration with other systems [31–33]. The following reaction sets represent the electrochemical and chemical reactions involved in the r-SOC system at 800 °C. The forward direction belongs to SOFC, and the backward direction characterizes SOEC [34].

$$H_2 + \frac{1}{2}O_2 \leftrightharpoons H_2O \quad \Delta h = -248.3\ \text{kJ mol}^{-1} \quad H_2\ \text{oxidation}/H_2O\ \text{reduction} \tag{1}$$

$$CO + \frac{1}{2}O_2 \leftrightharpoons CO_2 \quad \Delta h = -282.4\ \text{kJ mol}^{-1} \quad \text{CO oxidation}/CO_2\ \text{reduction} \tag{2}$$

$$H_2O + CH_4 \leftrightharpoons 3H_2 + CO \quad \Delta h = +206.3\ \text{kJ mol}^{-1} \quad \text{SMR/methanation} \tag{3}$$

$$H_2O + CO \leftrightharpoons H_2 + CO_2 \quad \Delta h = -34\ \text{kJ mol}^{-1} \quad \text{WGS/Rever}$$

2.1.1. Solid oxide electrolyzer cell (SOEC)

In H-O-C-based SOEC, the backward reactions in Eqs. (1)–(4) occur. High temperature co-electrolysis of H_2O and CO_2 as well as other chemical reactions in SOEC leads to syngas production and CO_2 mitigation [35,36]. Electricity could be supplied from intermittent RES to store the surplus generation. Heat demand for electrolysis reactions could be supplied externally by combustors or internally by exothermic methanation reaction and overpotential losses. Depending on the heat generation inside the SOEC due to losses or methanation reaction, the operation of the SOEC varies from endothermic to thermoneutral and exothermic mode [13]. In the SOEC, the fuel electrode is the cathode (reduction reaction site) and the air electrode is the anode [37].

2.1.2. Solid oxide fuel cell (SOFC)

Forward reactions mentioned in Eqs. (1)–(4) take place in H-O-C-based SOFC. Various types of fuel (H_2, syngas and hydrocarbons) could be utilized in SOFCs thanks to its broad range of operating temperature (750–1000 °C). Exothermic oxidation of fuels results in clean and silent electricity generation. The heat released in SOFC due to overall exothermic reactions and overpotential losses is absorbed by endothermic internal SMR and supplied air. Unlike SOEC, in SOFC the fuel electrode is the anode (oxidation reaction site) and air electrode is the cathode [37].

2.2. Thermal energy storage system (TES system)

Thermal energy storage is a technique to store heat in a medium at a required temperature for later consumption. It is an approach applied in RES to control instability of energy generation and consumption. The heat can be stored as internal energy in the heat transfer fluid (HTF) in sensible, latent, or thermochemical form. Sensible heat storage (SHS) systems employ the specific heat capacity, temperature change, and quantity of liquid or solid medium to charge and discharge thermal energy Eq. (5) [38]. Latent heat storage (LHS) systems, exploit the phase change heat concept, in which the storage material undergoes a phase transition during charging and discharging process Eq. (6). Due to rather low volumetric expansion and high enthalpy of phase change, solid-liquid a transition is more common technique [39,40]. The amount of storable heat in LHS is determined by mass and type of material (melting point, heat of fusion). The indices are explained in Table 9.

$$Q = \int_{T_i}^{T_f} \dot{m} C_p dT = \dot{m} C_p (T_f - T_i) \tag{5}$$

$$Q = \dot{m}[C_{ps}(T_m - T_s) + h + C_{pl}(T_l - T_m)] \tag{6}$$

2.2.1. Phase change materials (PCM)

PCMs are heat transfer media for the LHS technique. High energy storage density or high thermal inertia due to high phase change enthalpy makes the LHS an advantageous method. It furthermore provides a means of heat storage at a rather constant temperature thanks to isothermal phase transition phenomenon [41]. Selection of PCMs is based on thermophysical characteristics such as latent heat of fusion, thermal conductivity, density, and melting point. High enthalpy of fusion, thermal conductivity, density, and chemical stability are criteria that PCMs should meet. Depending on their melting point, PCMs are classified as low, intermediate and high temperature media [42].

2.3. Equilibrium reactor

A methanation reactor or Fischer-Tropsch system downstream the SOEC, makes it possible to improve syngas and produce desirable hydrocarbons such as methane, Dimethyl ether, and methanol. In this work, an equilibrium reactor using a proper Ni-based catalyst is utilized so as to operate a reversible methanation reaction. Therefore, depending on the operating condition of the reactor, either methanation or SMR occurs, Eq. (3) [43]. SMR reaction is highly endothermic and typically occurs at a temperature range of 800–1000 °C and a pressure of 10–30 bar over a nickel-based catalysts bed [44,45]. The reverse exothermic methanation reaction is highly favored at 300 °C and high pressure up to 20 bar over a nickel-based catalyst [46].

3. System configuration and component modeling

The aim of this research work lies in answering the following questions: is it feasible to build a system for energy storage based on r-SOC concept and what are the possible efficiencies that can be achieved? How pragmatic is it to achieve a thermally self-sustaining energy storage system relying solely upon the heat generations within the system? How can a TES system facilitate thermal management of the system without resorting to external heat sources such as furnaces? Which system configuration matches better the behavior of the commercially available r-SOC reactor and how it is influenced by key parameters such as pressure and current density? In order to answer the above-mentioned questions, an r-SOC process system was modeled using Aspen Plus® V8.8. A detailed description of the system architecture design and key components' modeling is provided in the following subchapters.

3.1. A reference system architecture

In order to analyze the model behavior, following assumptions were made within this study.

3.1.1. Assumptions

1. State of charge over one charge/discharge cycle is assumed to be equal; that is the number of oxygen ions being transferred through electrolyte is equal in oxidation (charging) and electrolysis (discharging) mode, Eq. (7).

$$q_{charging} = q_{discharging} \tag{7}$$

2. Duration of charging is assumed to be equal to discharging for simplification, Eq. (8).

$$t_{charging} = t_{discharging} \tag{8}$$

3. As a result of equal quantity and time of charge transfer, current flow through the circuit in both SOFC and SOEC mode is equal in magnitude but in opposite direction, Eq. (9).

$$I = qt \tag{9}$$

4. Composition of the fuel for any conditions is set such that the elemental ratios are met. This constraint is to provide enough hydrogen for carbon atoms enabling the methanation reaction ($\frac{H}{C} = 7.5$); and prevent coke formation inside the reactor and on components by sending enough steam or oxygen along with the fuel ($\frac{O}{C} = 2.5$) [47].
5. It is supposed that chemical reactions occurring in the SOC, methanation and SMR reactors reach equilibrium and that the outlet gases are at equilibrium at the given pressure and temperature.
6. The boundary conditions of the system and design specifications of the BOP are provided in Tables 1 and 2, respectively.

3.1.2. Process system description during charging mode or SOEC operation

The process scheme of the r-SOC system during SOEC mode is shown in Fig. 3. In this process, gas from exhaust tank mainly composed of carbon dioxide is expanded to system pressure from its storage pressure, 25 bar. The required water which is stored at atmospheric pressure and 90 °C is pumped to the evaporator and superheater units. The superheated steam is then mixed with the process gas from the exhaust tank. The resultant stream is sent to the heat recovery units to be preheated. In order to bring the temperature of the gas stream to the required inlet conditions of the SOEC reactor, the gas is directed to low and high temperature heat storage tanks, respectively. Heat stored in the storage tanks is absorbed by the inlet/

Table 1
Boundary conditions of r-SOC system at reference condition.

	Pressure in bar	Temperature in °C
Fuel storage tank	25	110
Exhaust storage tank	25	110
Water storage tank	1	90
SOC in FC mode	1	850
SOC in EC mode	1	800
High-temperature storage tank	1	850
Low-temperature storage tank	1	750
SOFC inlet air	1	700
SOFC inlet fuel	1	750
SOEC inlet streams	1	820

Temperature gradient over the reactor 50 °C $\leqslant \Delta T \leqslant$ 200 °C .

Table 2
Design condition for BOP.

Heat exchanger pinch point temperature in °C	10
Compressor isentropic and mechanical efficiency in %	85
Expander isentropic and mechanical efficiency in %	85
Current density of r-SOC reactor in $A\ cm^{-2}$	0.25

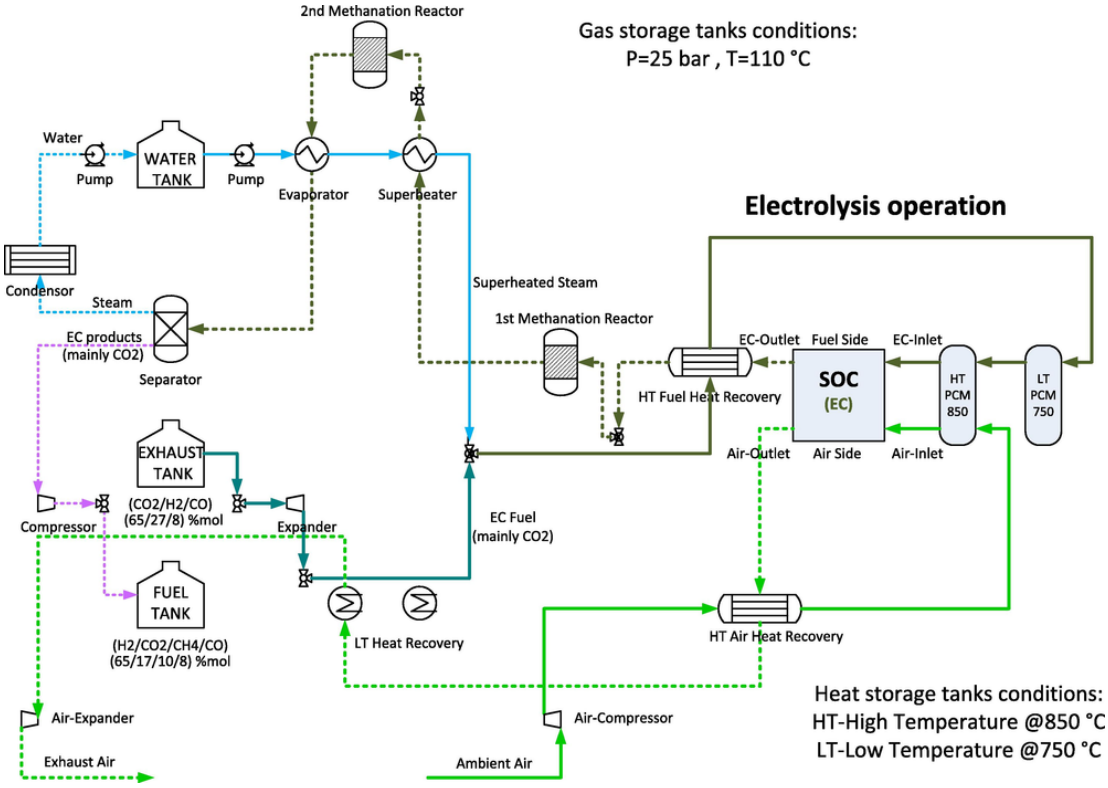

Fig. 3. Process flow diagram for r-SOC system in charging/electrolysis mode (SOEC); solid lines: reactant streams, dashed lines: outlet streams.

reactant streams and temperature reaches the required value. Besides, air is supplied from ambient to the system for two reasons; firstly, it flushes out the produced oxygen from electrolysis reactions of SOEC; secondly, it acts as a medium that carries heat to or from the r-SOC reactor to meet the boundary conditions. It is first preheated in the air heat recovery unit and then directed to the high temperature storage tank (HT-ST). In HT-ST, both streams absorb heat to reach boundary conditions for the SOEC inlet temperature. Both air and process gas leave the HT-ST at 820 °C and enter to the air and fuel channel of the r-SOC reactor respectively. Water and carbon dioxide in reactants undergo electrolysis reactions inside the SOEC reactor at an average reactor temperature of 800 °C. Due to presence of suitable catalyst, further chemical reactions such as internal methanation and RWGS reaction also occur in SOEC (Eqs. (3) and (4)). As a consequence of all reactions, the produced H_2 and syngas leave the fuel channel and air stream with additional oxygen content leaves the air channel of the r-SOC. Both streams exit the r-SOC at 648 °C and are sent to the heat recovery units to preheat the inlet streams. Product gas exits the heat recovery unit at 380 °C and enters a double-stage methanator unit. The heat generated due to exothermic methanation reactions is employed in the superheater and evaporator unit for steam generation. The final fuel product, now higher in methane content, is separated from the steam, compressed and brought to fuel storage tank condition. Separated steam on the other hand, is condensed and cooled down to 90 °C and pumped into the water tank. The outlet air stream from the r-SOC reactor is vented to ambient pressure after being cooled down in heat recovery unit.

3.1.3. Process system description during discharging mode or SOFC operation

The process scheme of the r-SOC system during SOFC operation is shown in Fig. 4. In this process, the fuel gas produced during SOEC mode is employed to generate heat and electricity. The fuel gas (mainly H_2) is expanded from the fuel storage tank to system pressure. It is first preheated in the low temperature heat recovery unit and then mixed with the superheated steam. Steam is added to the reactant stream to prevent coke formation and promote steam methane reforming (SMR) reaction. The consequent mixture of fuel gas and steam is directed to an equilibrium reactor. The outlet gas mixture enters the heat recovery unit to reach required inlet temperature of 750 °C for SOFC . The required oxygen for oxidation reactions is supplied from ambient air after being heated to 700 °C in air the heat recovery unit. The mass flow of air is controlled to cool the SOFC and maintain outlet temperatures at boundary condition level. Fuel and air enter the fuel and air channel of the r-SOC respectively and undergo the forward reactions in Eqs. (1)–(4). Under fuel cell operations, air with lower content of oxygen leaves the air channel and exhaust gas mainly composed of steam, carbon dioxide and unreacted fuel leaves the fuel channel of the r-SOC at 890 °C. High quality heat within these streams is first stored in the HT-ST at 850 °C and afterwards in the LT-ST at 750 °C. The remaining heat in outlet streams is utilized by the inlet streams in heat recovery units. Finally, the steam content of the exhaust gas is separated, condensed and stored in the water tank. The remaining exhaust gas predominated by CO_2 is compressed and kept in the exhaust storage tank. Outlet air is emitted to ambient after being cooled down in the heat recovery unit.

3.2. Component modeling

The detailed description of methods and assumptions used for component modeling is presented in the following subchapters.

Table 3
Summary of melting point and heat of fusion for potential components as PCM.

Composite	Melting point °C	Heat of fusion (kJ/kg)
70% LiF + 30% MgF_2	728	520
65% NaF + 23% CaF_2 + 12% MgF_2	743	568
67% LiF + 33% MgF_2	746	947
74% LiF + 13% KF + 13% MgF_2	749	860
80% LiF + 20% CeF_3	756	500
81.5% LiF + 19.5% CaF_2	769	820
85% KF + 15% CaF_2	780	440
85% KF + 15% MgF_2	790	520
64% NaF + 20% MgF_2 + 16% KF	804	650
62.5% NaF + 22.5% MgF_2 + 15% KF	809	543
68% NaF + 32% CaF_2	810	600
75% NaF + 25% MgF_2	832	627
LiF	848	1080
KF	856	486
40% NaF + 40% MgF_2 + 20% CaF_2	914	590
49% CaF_2 + 41.4% $CaSO_4$ + 9.6% $CaMoO_4$	943	237

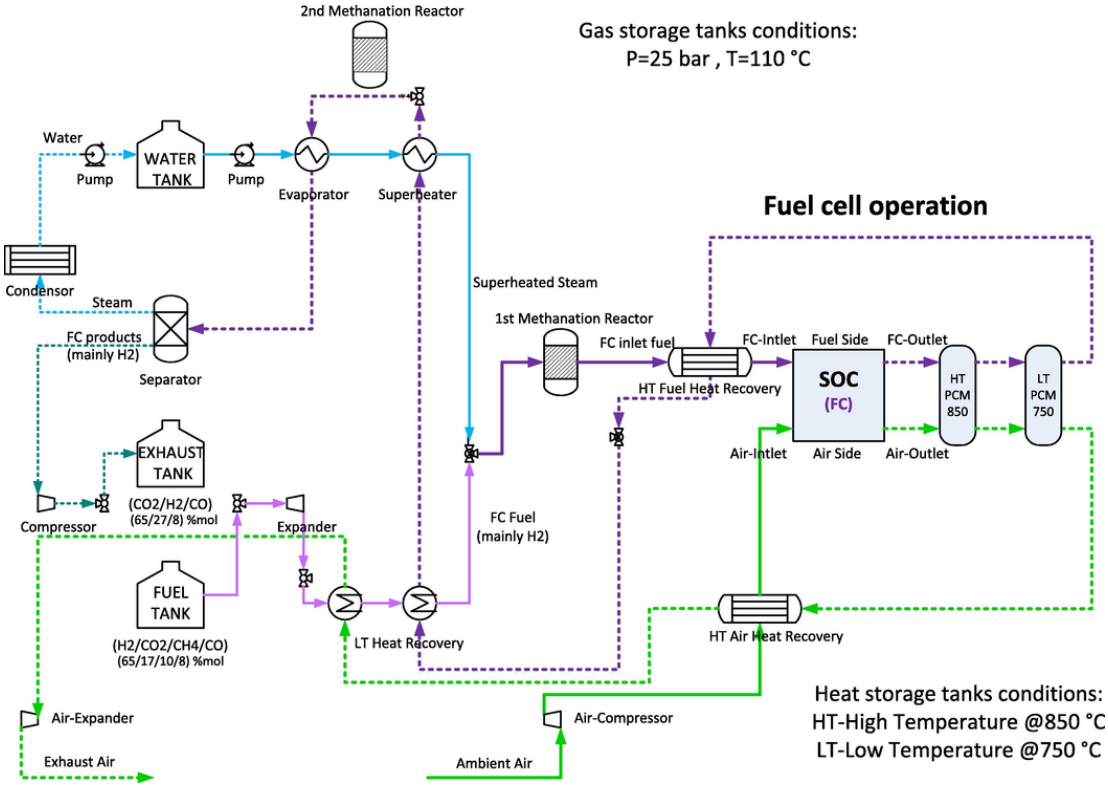

Fig. 4. Process flow diagram for r-SOC system in discharging/fuel cell mode (SOFC); solid lines: reactant streams, dashed lines: outlet streams.

3.2.1. r-SOC

The r-SOC model used in this work is based on a commercially available r-SOC reactor with a planar design. Being an ESC type SOC reactor, it is characterized by a thick electrolyte and thin electrodes. The 10-cell planar r-SOC reactor was experimentally characterized using DLR's pressurized test rig facility. Based on the experimental results a semi-empirical temperature dependent ASR model is developed and used in this work. A temperature based function for ASR is justified for the ESC reactor since from the experiments it was found that ohmic resistance was the dominating loss mechanism owing to the thick electrolyte, Eq. (15). Ohmic resistance is dependent on temperature and not on pressure [48]. In this work, r-SOC reactor is developed in Aspen Plus® as a hierarchical block that incorporates all features and behavior of a SOFC and SOEC unit, though in an entirely individual approach. Implementation of the model in Aspen can be found in Appendix A. Mass and energy conservation over the r-SOC reactor in steady state condition are considered as in Eqs. (10) and (11). The indices are explained in Table 9.

$$\dot{m}_{pg,in} + \dot{m}_{air,in} = \dot{m}_{pg,out} + \dot{m}_{air,out} \tag{10}$$

$$\dot{m}_{pg,in} \cdot h_{pg,in} + \dot{m}_{air,in} \cdot h_{air,in} + P_{rSOC} = \dot{m}_{pg,out} \cdot h_{pg,out} + \dot{m}_{air,out} \cdot h_{air,out} \tag{11}$$

where the mass flow rate of the process gases (either SOFC or SOEC) entering and leaving the reactor is respectively denoted by $\dot{m}_{pg,in}$ and $\dot{m}_{pg,out}$. $\dot{m}_{air,in}$ and $\dot{m}_{air,out}$ denote the mass flow rate of air entering and exiting the reactor. The term P_{r-SOC} is a general term for power; it could be negative as a product of fuel cell operation P_{SOFC} or positive as a supplied power for electrolysis reactions P_{SOEC}. The methodology of developing each unit within the r-SOC including SOFC and SOEC is provided in the followings.

For the SOFC mode the RGibbs reactor model is used to simulate fuel chamber (anode) and the chemical reactions inside the SOFC. A separator is used to simulate the oxide-ion conducting electrolyte. The mass of oxygen ions transferred is calculated externally in Fortran code. A heater is used to simulate the internal heat transfer. For the SOEC operation, the inlet reactant gas is first brought to equilibrium in REquil reactor. Electrochemical reduction of H_2O and CO_2 is simulated in the RStoic reactor for a given extent of the reaction. Likewise, in the SOFC a separator is used to model the electrolyte to remove the oxygen from the fuel stream and supply to the air stream. The products of the RStoic reactor are finally brought to equilibrium in the RGibbs reactor to simulate other chemical reactions such as internal methanation, etc. The electrochemical model to calculate reactor voltage, power, oxygen ion transfer, and current is modeled in an external Fortran block.

3.2.2. Electrochemical model

The electrochemical model is implemented in an external Fortran-based calculator block. The Nernst (ideal) voltage is calculated based on Gibbs free energy of H_2 oxidation (H_2O reduction) which depends on conversion of the reaction, temperature and pressure. The outlet compositions are used for calculating the Nernst voltage in Eq. (12). [49,50]. The standards Gibbs free energy of reaction (ΔG°) is calculated from Eq. (13) [51]. The electrochemical losses are implemented based on a lumped resistance model. The ASR model was obtained from experimental results , Eq. (14) [52]. The final operating voltage of a single cell in the r-SOC reactor is calculated from Eq. (16) considering overpotential loss effect (positive for SOEC, negative for SOFC). The heat released or consumed by the r-SOC reactor

is obtained from Eq. (18) based on thermodynamics' first law in fuel cells. The heat calculated is inclusive of the heat produced due to electrochemical losses.

$$V_{Nernst} = \frac{-\Delta G^{\circ}}{P\bar{z}\cdot F} - R\frac{T_{SOFC}}{\bar{z}\cdot F}\ln\left(\frac{p_{H_2O}}{p_{H_2}\cdot (p_{O_2})^{0.5}}\right) \quad (12)$$

$$\Delta G^{\circ} = 246000 - 54.8.T_{SOC} \quad \frac{J}{mol} \quad (13)$$

$$ASR = 0.30813 + 767370.\exp\left(-0.013295.T_{SOC}\right) \quad \Omega cm^2 \quad (14$$

$$V_{loss} = J.ASR \quad (15)$$

$$V_{cell} = V_{Nernst} \pm V_{loss} \quad (16)$$

$$P_{SOC} = V_{cell}\cdot I_{SOC} \quad (17)$$

$$\dot{Q}_{SOC} = \Delta\dot{H}_{rxn,SOC} - P_{SOC} \quad (18)$$

The reactor current and oxygen ions transferred are calculated based on the equations below. The maximum current for electrochemical oxidation in SOFC and reduction in SOEC mode is given by Eqs. (19) and (20), respectively. The actual cell current is a product of maximum current and utilization value. The oxygen ions transferred is then calculated from reactor current via Faraday's law.

$$I_{max,SOC} = (8\dot{n}_{CH_4} + 2\dot{n}_{H_2} + 2\dot{n}_{CO})\cdot F \text{ in SOFC mode} \quad (19)$$

$$I_{max,SOC} = (\dot{n}_{H_2O} + 2\dot{n}_{CO_2})\cdot 2\cdot F \text{ inSOEC mode} \quad (20)$$

$$I_{SOC} = U_{f,SOC}I_{max,SOC} \quad (21)$$

$$\dot{n}_{O_2} = \frac{I_{SOC}}{2\bar{z}F} \quad (22)$$

3.2.3. Heat storage

In this system, TES is implemented using latent a heat thermal energy storage (LHTES) technique. The working principle behind LHTES is releasing or absorbing heat in an almost isothermal process. This heat exchange leads to phase transition of the storage material. The model is therefore based on the fundamental mass and energy balance formulas for heat exchange between streams and PCMs.

$$\sum_{in}\dot{m}_i - \sum_{out}\dot{m}_i = 0 \quad (23)$$

$$\sum_{in}h_i\ \dot{m}_i - \sum_{out}h_i\ \dot{m}_i = \dot{Q}_{storage} \quad (24)$$

$$\dot{Q}_{storage} = \dot{m}_{PCM}[C_{ps,PCM}(T_{m,PCM} - T_{s,PCM}) + h_{PCM} + C_{pl,PCM}$$

The implementation of LHTES unit in Aspen Plus® is not straightforward both from material and component viewpoint. The following steps are exerted in Aspen Plus® to simulate LHTES.

- A thermal energy storage tank is considered as a 2-stream-heat-exchanger.
- Due to its higher energetic and exergetic efficiency, a cascade model of latent heat storage unit is designed. Therefore, the process of heat storage/consumption takes place in a 2-stage heat storage unit. One stage is considered to be HT-ST at 850 °C and the other is LT-ST at 750 °C.
- The storage material or PCM for each stage is selected such that its melting point is very close to the storage temperature.
- Fluoride salts are found to have suitable melting points T_m range (700-950 °C) for this study [53,54].(see Table 3)
- LiF with a T_m = 848 °C is employed as PCM for HT-ST, while a fluoride salt (74% LiF + 13% KF + 13% MgF_2) with T_m = 749 °C is considered to be PCM in LT-ST.
- However, since the exact material model of this composite is not available steam is used in the implementation of LHTES in Aspen Plus® instead of PCM. This does not affect the model and system performance, as long as the temperature difference of the process stream, temperature of heat storage medium and quantity of heat transfer are maintained [55].

3.2.4. Equilibrium reactor (SMR-Methanation)

The external SMR and methanation reactions Eq. (3) are considered to reach adiabatic equilibrium at the reactor conditions. Therefore, an equilibrium reactor in Aspen Plus® named RGibbs is chosen for simulating these reactions at adiabatic conditions. This reactor is considered to be equipped with a Ni-base catalyst suitable both for the SMR and methanation reactions. The minimum temperature either at the inlet or outlet of reactor is set to be 380 °C. This temperature restriction is set to due to the inactivity of the Ni-based catalyst at lower temperatures. . Depending on the conditions such as temperature, pressure and reactant/product concentrations the SMR reactions can shift to forward direction or reverse direction. In other words, the same reactor used for the methanation reaction in SOEC mode can operate as SMR reactor in SOFC mode as long as the required conditions are met. This is due to the primarily Ni-based catalyst that is same for SMR and methanation reactions [56,57]. To improve the methane formation, two methanation reactors are employed to act as a 2-stage methanator. The pressure of equilibrium reactor changes according to the system pressure. Hence for the reference case it is set at 1 bar.

4. Results and discussion

Key results of the process system model simulation for reference case and impact of key operating parameters on its performance are discussed in this chapter. In order to have a better understanding of the system behavior and performance, some non-dimensional parameters have been introduced. These indicators are defined in the following part.

- Round-trip efficiency (η_{RT}): It is an indicator of performance for the system and the r-SOC reactor. For r-SOC reactor, it is the ratio of the generated electrical power by oxidation in SOFC mode P_{SOFC} to the consumed electrical power for electrolysis in SOEC mode P_{SOEC}, Eq. (26). In the system level, the round-trip efficiency also incorporates the parasitic power consumption incurred by balance of plant (BOP) components, Eq. (27). Sign convention is in Table 9.

$$\eta_{RT-reactor} = \frac{P_{SOFC}}{P_{SOEC}} \tag{26}$$

$$\eta_{RT\_system} = \left| \frac{P_{SOFC} + \sum P_{BOP,SOFC}}{P_{SOEC} + \sum P_{BOP,SOEC}} \right| \tag{27}$$

- Relative BOP power ($RelativeP_{BOP}$): It is a non-dimensional parameter that compares the total electrical power belonging to BOP with the power associate to r-SOC in each mode of operation. Therefore $RelativeP_{BOP,SOFC}$ represents the ratio of total BOP power to the produced power from the r-SOC reactor during SOFC operation and $RelativeP_{BOP,SOEC}$ indicates the ratio of total BOP power to the power consumed by the r-SOC reactor during SOEC operation, Eqs. (28) and (29).

$$RelativeP_{BOP,SOFC} = \frac{\sum P_{BOP,SOFC}}{P_{SOFC}} \tag{28}$$

$$RelativeP_{BOP,SOEC} = \frac{\sum P_{BOP,SOEC}}{P_{SOEC}} \tag{29}$$

- Alpha (α): This parameter is defined to demonstrate the thermal performance of the system during its SOEC mode. Depending on endothermic/exothermic behavior of the electrolyzer, Q_{SOEC} could be the heat required for/generated from SOEC. Based on the sign convention, Q_{SOEC} is positive for endothermic and negative for exothermic mode of SOEC. α is the ratio of Q_{SOEC} to the total heat consumption from both high and low thermal energy storage tanks Q_{Cons}. Hence, the positive sign of α implies the endothermic mode of SOEC and the negative sign indicates its exothermic mode.

$$\alpha = \frac{Q_{SOEC}}{Q_{Cons}} \tag{30}$$

4.1. A reference case

The reference case is set based on the conditions given in Table 4.

The compositions of process gases in fuel and exhaust tanks are at steady-state condition. These compositions are obtained after several consecutive operations of system in SOFC and SOEC mode. Once the composition of each tank after a complete cycle of charging/discharging reaches to its initial value and does not vary, the system is at steady state condition. At this condition, the product gas from the SOFC mode is the reactant gas for the SOEC mode and the product of the SOEC mode after methanation process is the reactant gas for the SOFC mode. Table 5 shows the composition of the process gas in discharging mode at different levels: before entering the system (fuel tank), after mixing with steam (SOFC inlet), after all reactions (SOFC outlet, wet), and after separation from st $U_{f,SOEC}$ eam (SOFC outlet, dry).

Table 6 shows the composition of the process gas in the same points in charging mode. The product of the SOFC mode is utilized as reactant of the SOEC mode as could be seen from equal values in Table 5 and Table 6. In all conditions, the criteria for minimum H/C and O/C are met.

A summary of the key results for the system performance in the reference case are shown in Table 7. The utilization factor in electrolysis mode is calculated based on assumption of equal current in SOFC and SOEC mode. The performance indicators is illustrated in Figs. 5-7.

Fig. 5 depicts the performance of the system when it operates in the SOFC mode. Based on this pie chart, out of 100 units of chemical power in fuel that is being sent to the SOFC, 47.6 units are converted to electricity, 6.9 units are stored as heat in the HT-ST and 15.8 units are stored in the LT-ST. The remaining heat inside the gas streams amount to 8.9% of chemical power of inlet fuel stream and could be exploited in the heat recovery units. 20.8 units of the chemical power are neither converted to electricity nor heat inside SOFC. This sector represents the portion of the initial fuel that did not participate in any SOFC reactions and hence remained in form of chemical power in the gas stream.

Effectiveness of the thermal energy storage tanks are illustrated in Fig. 6. The process gasses going into the r-SOC reactor during the SOEC mode first pass through the LT-ST at 750 °C. By absorbing 81.7% of the available heat, the process gases exit the LT-ST at 744 °C. This temperature is not high enough to meet the boundary condition of the SOEC reactor. In order to reach 820 °C the gases pass through the HT-ST at 850 °C and absorb almost 100% of the stored heat, as observed in Fig. 6. This heat is carried to the r-SOC reactor during SOEC operation mode to offset the heat requirement for endothermic reactions. As shown in the third bar, in total 86.8% of the heat stored in both TES tanks was used by inlet process gases for SOEC mode. The distribution of absorbed heat from the TES tanks for preheating and endothermic requirements of SOEC reactor is shown in Fig. 7.

According to Fig. 7, only 41.4% of the heat stored in the TES tanks system is enough to compensate the heat demand for endothermic reaction in SOEC. 58.6% of the absorbed heat is indeed used for preheating the streams. This implies the significant role of the TES system in thermal management of the system.

Other noteworthy result of the reference case is the functionality of an external equilibrium reactors inside the system. As mentioned earlier in Section 3.2.3, the equilibrium reactor can either act as a methanator or as reformer depending on conditions such as temperature, pressure, composition. In SOEC mode, it always operates as a methanator because of the low inlet temperature that is always reduced to 380 °C and also because of the favorable composition (higher H_2 and CO) for the methanation reaction. In SOFC, the inlet temperature is determined by the available heat in the heat recovery unit before the equilibrium reactor. At the reference case this temperature does not go beyond 424 °C. The temperature is not high enough to prompt the endothermic SMR and also due to low CH_4 content in fuel, methanation takes place before SOFC. As a result, the outlet stream is richer in methane content and the temperature is increased. This interesting result is contrary to most conventional SOFC systems integrated with an external reforming reactor. The equilibrium reactor which acts as methanator plays an important role in obtaining a thermally self-sustaining system in the SOFC mode. The reason is the exothermic nature of the methanation reaction that increases the temperature of process gas by more than 100 degrees. As a result of

Table 4
Reference case condition.

p	1 bar
J	0.25 A cm^{-2}
$U_{f,SOFC}$	85%

Table 5
Process gas molar compositions (%) in SOFC mode.

Component	Fuel tank	SOFC inlet (Wet)	SOFC outlet (Wet)	SOFC outlet (Dry)
H_2	65.2	44.8	7.8	27.0
H_2O	0.00	31.2	71.2	0.00
CO	7.80	5.4	2.5	8.6
CO_2	16.9	11.7	18.5	64.4
CH_4	10.1	6.9	0.00	0.00

Table 6
Process gas molar compositions (%) in SOEC mode.

Component	Exhaust tank	SOEC inlet (Wet)	SOEC outlet (Wet)	SOEC outlet (Dry)
H_2	27.0	7.8	44.8	65.2
H_2O	0.00	71.2	31.2	0.00
CO	8.6	2.5	5.4	7.8
CO_2	64.4	18.5	11.7	16.9
CH_4	0.00	0.00	6.9	10.1

Table 7
Summary of reference case results.

Performance indicator	Value in%
$\eta_{RT\_reactor}$	56.3
η_{RT_system}	54.3
$U_{f,SOEC}$	65
α	41.4

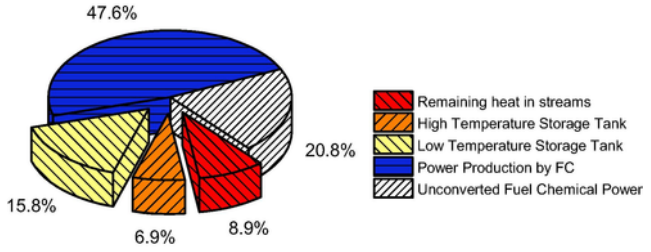

Fig. 5. Distribution of chemical power in fuel to other forms of power during SOFC mode.

this temperature rise, less amount of heat is required to be absorbed from the SOFC outlet streams at heat recovery units. Since less heat is required at the heat recovery units from the SOFC outlet streams, more amount of heat could be stored in the TES tanks which could be later utilized for the SOEC mode heat demands. This means that no external heat source such as combustor or electric heater is required to bring the streams to the system boundary conditions. Although the exothermic methanation reaction is beneficial for thermal management of the system, the conversion of hydrogen's chemical energy to heat as a result of the methanation reaction causes an exergy loss. More simply, the inlet fuel to the SOFC reactor after the methanation reactor has less exergy than the inlet fuel that has not passed the methanation reactor resulting in a lower round-trip efficiency.

4.2. Parametric analysis

In order to investigate the effect of key parameters on the system behavior, two parametric analyses was performed on this system: variation of current density and pressure. In the former, current density is changed from 0.20 to 0.45 $\mathrm{A\ cm^{-2}}$ while keeping the other variables of the system unchanged. In the latter, the pressure of system is increased from atmospheric condition to 25 bar. The following sections explain the effects on system through key performance indicators.

4.2.1. Current density effect (J)

As J was increased from 0.20 to 0.45 $\mathrm{A\ cm^{-2}}$, many V_{cell} system indicators changed consequently. The effect of current density on round-trip efficiency is given in Fig. 8.

According to Fig. 8, as J increases, $\eta_{RT\_reactor}$ drops from 60.3% to 41.6%. Decline of $\eta_{RT\_reactor}$ which is defined in Eq. (26) is due to the effect of the current density on the overpotential loss and subsequently on the power production/consumption of the r-SOC reactor. As shown in Eq. (17) P_{SOFC} and P_{SOEC} are linearly proportional to V_{cell} and I in respective mode. As per Eq. (15), V_{loss} rises as J rises. Therefore, as J increases of V_{cell} of the SOFC decreases whereas V_{cell} of the SOEC increases. Hence, as J increases, P_{SOFC} decreases and P_{SOEC} increases reducing the roundtrip efficiency. The heat loss issuing from h η_{RT_system} higher current density pushes the SOEC operation towards an exothermic behavior. V_{cell} of SOEC increases from 1.15 V at J = 0.2 $\mathrm{A\ cm^{-2}}$ and reaches 1.34 V at J = 0.45 $\mathrm{A\ cm^{-2}}$. The intersection of V_{cell} with V_{TN} is where the SOEC reactor reaches its thermoneutral point and enters exothermic mode. Therefore, it is concluded that the SOEC reactor reaches its thermoneutral point at J = 0.4 $\mathrm{A\ cm^{-2}}$.

A similar descending trend is observed in behavior of η_{RT_system} in response to J variation. The only difference is the lower magnitude of which is because of the BOP consumption. It reduced from 58.1% to 40.6% as J was varied from 0.2 to 0.45 $\mathrm{A\ cm^{-2}}$, and the reason behind that is the same as the reason for $\eta_{RT\_reactor}$ drop. This means that in this system current density does not affect the BOP consumption.

The effect of current density on the thermal management of the system during SOEC mode could be perceived from dimensionless indicator α. As defined in the introduction of Section 4 the relation between Q_{SOEC} and heat consumption from the TES tanks (Q_{Cons}) in charging mode of the system is represented by α. Q_{SOEC} could be either the heat required for the SOEC for endothermic reactions or the heat released from it after entering into the exothermic mode. As J moves towards higher values, α decreases and moves towards the exothermic region as shown in Fig. 9. This descending trend is attributed again to effect of J on V_{loss}. The higher J, the higher overpotential loss generated inside the r-SOC reactor both in SOEC and SOFC mode. This means more heat generation in the SOFC mode and thereby more heat storage in the TES tanks. Consequently, more heat is available in the TES tanks for endothermic operation of the SOEC mode. In the SOEC mode, the heat generated by overpotential losses can itself meet the heat demand for the endothermic reactions and therefore less heat is required to be consumed from the TES. Fig. 9 demonstrates that as J increases less portion of Q_{Cons} is used to support the heat demand inside the SOEC reactor. The ratio of Q_{SOEC} to Q_{Cons} decreases from 49.9% at J = 0.2 $\mathrm{A\ cm^{-2}}$ to −34.8% at J = 0.45 $\mathrm{A\ cm^{-2}}$. The intersection of α graph with the abscissa at J = 0.4 $\mathrm{A\ cm^{-2}}$ indicates the thermoneutral point of the SOEC and the negative sign of α signifies the exothermic operation of it. The noteworthy point of this figure is the fact that the TES tanks are still essential part of

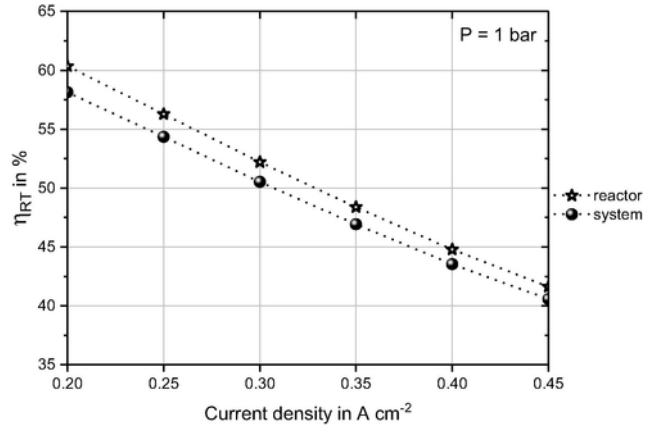

Fig. 8. Effect of current density on round-trip efficiency of reactor and system.

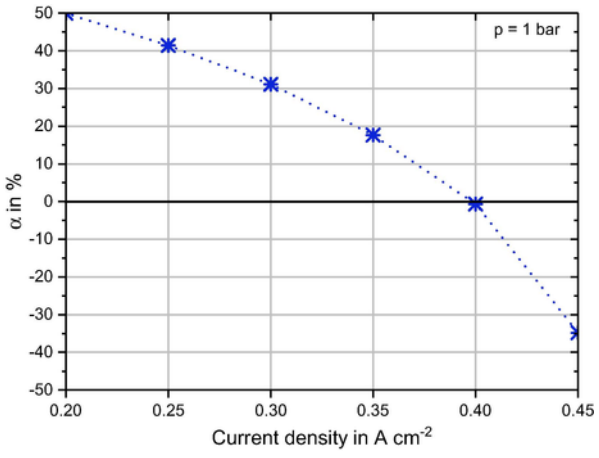

Fig. 9. Effect of current density on thermal management of system in SOEC mode.

the SOEC system even though it enters its exothermic mode. To put it simply, the heat generated by exothermic behavior of the SOEC is not yet sufficient to preheat the inlet gas streams even at a high current density value of J = 0.45 $A\ cm^{-1}$. In other words, the integration of the TES systems is vital for the SOEC system even in its exothermic mode because of its significant role in preheating the reactant streams. Only when α reaches about −100% and beyond we can assure that heat generation by exothermic SOEC operation is adequate to also preheat the inlet streams to the SOEC. To reach $\alpha = -100\%$ the current density should be raised to a very high value, which impairs η_{RT} and reduces it to a very low value. It could be concluded that it is more reasonable to operate the SOEC system in endothermic mode and keep the TES unit as an essential component in the SOEC system for thermal management.

4.2.2. Pressure effect

Pressurization effect on the system behavior will be provided in this section. The system pressure is increased from 1 bar to 25 bar and the impact on different aspects of the system were studied and presented in the following.

The impact of the pressure on the round-trip efficiency for both the r-SOC reactor and the system are shown in Fig. 10. Pressurization has a beneficial effect on the r-SOC reactor as shown by an ascending trend of $\eta_{RT-reactor}$ in Fig. 10. As p increases from 1 bar to 25 bar $\eta_{RT\_reactor}$ grows from 56.3% to 60.5%. According to Eq. (26), $\eta_{RT\_reactor}$ merely depends on variation of the power for both modes: P_{SOFC} and P_{SOEC}. Since electrical power is linearly proportional to V and J, the impact of p is investigated on them. The effect of pressure on the voltage is shown in Fig. 11. An increase of p leads to an increase of V_{Nernst} and consequently V_{cell} during the SOFC mode. Likewise, it results in a rise of V_{Nernst} and V_{cell} during the SOEC mode. Since the r-SOC reactor in this system is a ESC type, the effect of pressure on the ASR is negligible [52]. Average temperature of the reactor is maintained fixed, so the ASR remains constant Eq. (14). Current density is kept constant at J = 0.25 $A\ cm^{-2}$ as p increases. Hence V_{loss} does not vary by p which is also observable in Fig. 11 where the difference between V_{Nernst} and V_{Cell}, or $\eta_{overpotential}$ is always constant for both modes. According to Eq. (12), the second term in V_{Nernst} is a function of the pressure. As pressure increases V_{Nernst} also increases in both SOFC and SOEC mode. This effect is direct consequence of thermodynamics. Consequently, V_{Cell} in both SOEC and SOFC mode increases; this means that a higher pressure has a positive effect on the fuel cell but a negative effect on the electrolysis cell. Overall, the beneficial effect of high pressure on the fuel cell operation overcomes the detrimental effect of it on the electrolysis operation leading to an improved $\eta_{RT\_reactor}$.

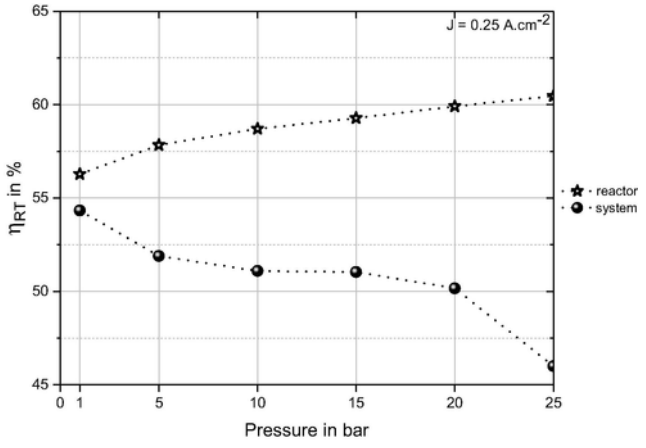

Fig. 10. Effect of pressure on round-trip efficiency of reactor and system.

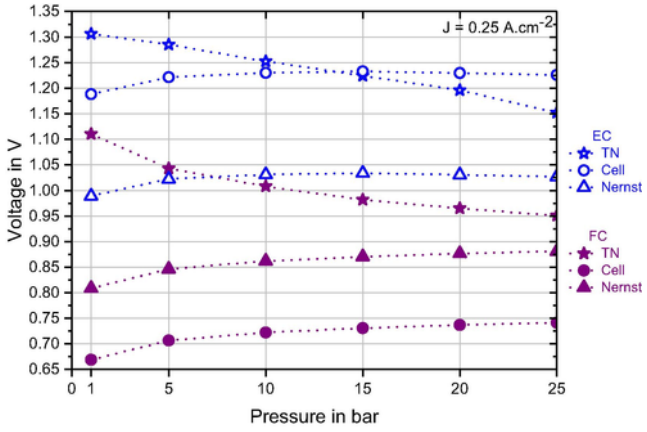

Fig. 11. Variation of voltage with pressure.

On the other hand, the effect of high pressure on η_{RT_system} is not as promising as $\eta_{RT\_reactor}$. It declines from 54.3% to 46%. Although the r-SOC reactor has a better performance at higher pressure, the entire system cannot benefit from it. This downtrend in η_{RT_system} is attributable to high power consumption of BOP at higher pressures. In particular, the power required for the air compressors from ambient to system pressure. In order to see the effect of pressure on the BOP, non-dimensional parameters namely $RelativeP_{BOP,SOFC}$ and $RelativeP_{BOP,SOEC}$ are plotted in Fig. 12. The y-axis of this plot displays the ratio of net BOP power to the r-SOC reactor power corresponding to each mode. Based on the sign convention provided in Table 9 the power production is regarded to a have negative sign and the power consumption is regarded as positive. Nevertheless, in Fig. 12 the denominator (P_{SOFC} or P_{SOEC}) is considered to be the absolute value while the nominator is the net sum of the power consumption/production by BOP components. Therefore, the positive value in Fig. 12 means that the net BOP power is positive and the system is consuming power whereas the negative value means that net BOP power is negative and the system is generating power in that mode. At 1 bar in SOFC mode, the net BOP power is -1.4% of absolute P_{SOFC}. This demonstrates that the BOP components in the SOFC mode at 1 bar are indeed producing power and that this effect is due to the fuel expander which expands the fuel from the

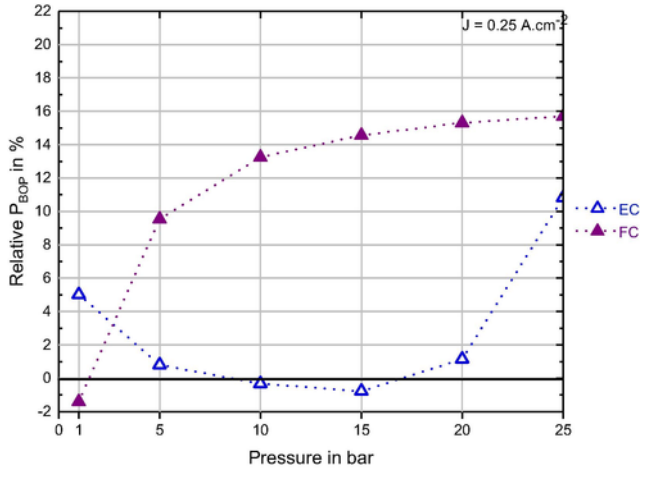

Fig. 12. Effect of pressure on BOP.

storage tank at 25 bar to the system pressure at 1 bar. However, at the same pressure, net BOP power in the SOEC mode is 5% of P_{SOEC} meaning that the system is consuming parasitic BOP power in SOEC mode along with required power for electrolysis. In general, at 1 bar the system consumes BOP power and which is the reason of lower η_{RT_system} than $\eta_{RT\_reactor}$. The ratio of the BOP power to P_{SOFC} increases as the p goes up from 1 to 25 bar. At 25 bar, $RelativeP_{BOP,SOFC}$ reaches 15.7% because of high pressure ratio in the air compressor. A noteworthy point of this graph in the SOFC mode is the dramatic increase in relative BOP from 1 to 5 bar. The plot reduces with a smoother slope as p increases. This behavior is due to the methanation reaction which is favored at higher pressures. Since more methane is produced in electrolysis mode both inside electrolyzer and in methanation reactors, the produced gas from SOEC mode contains more percentage of methane at higher pressures as shown in Fig. 13. The produced gas from SOEC is stored in the fuel tank and sent to the system during SOFC mode as fuel. Owing to higher contents of methane in fuel stream in SOFC mode, internal SMR reaction in the SOFC moves more towards forward direction, Eq. (3). Since SMR is an endothermic reaction, it absorbs the heat produced in the SOFC and acts like a coolant for the r-SOC reactor in SOFC mode. Thus, less amount of air is required for the SOFC reactor for cooling purpose at higher pressures. Less quantities of air leads to less compression work consumption by the air compressors. The reason of an incremental trend for $RelativeP_{BOP,SOFC}$ with a lower slope at higher pressure is the lower mass flow rate of air entering the compressor in SOFC mode. On the other hand, the trend of $RelativeP_{BOP,SOEC}$ is different from $RelativeP_{BOP,SOFC}$. The reason is again the pressure effect on methanation reaction. As pressure increases, reaction Eq. (3) moves backwards (methanation) which has an exothermic nature. This means that higher amount of heat is produced inside the r-SOC reactor in SOEC mode as pressure goes up. Therefore, less amount of air is required for the SOEC reactor as heating agent for endothermic reactions. The decreasing trend of $RelativeP_{BOP,SOEC}$ from 1 to 15 bar is owing to less amount of air compressor work as a result of low air flow rate. The drastic increase of $RelativeP_{BOP,SOEC}$ from 15 to 25 bar is an indication of an exothermic behavior of the SOEC reactor. As shown in Fig. 11, the intersection of V_{cell} and V_{TN} occurs at pressure close to 15 bar meaning that the SOEC reaches its thermoneutral point at this pressure and enters its exothermic mode at pressures above this value. In order to keep the r-SOC reactor in its boundary conditions, more air is required to cool down the SOEC reactor when it enters the exothermic mode. Thus, the amount of air sent to the SOEC at pressures higher than 15 bar has noticeably increased and results in a higher work of air compressor. This leads to a steep decline of η_{RT_system} from 15 to 25 bar.

The effect of pressure on thermal management of the system during SOEC mode could be understood from the α factor. As mentioned earlier, α represents the ratio of heat required/produced by SOEC reactor to the heat absorbed from both high and low temperature heat storage systems. The denominator (heat consumption from TES tanks) is always positive while the nominator is positive for endothermic and negative for exothermic behavior of the SOEC. As pressure rises from 1 to 25 bar (see Fig 14), α varies from 41.4% to −58.6%; this implies that by increasing pressure the behavior of the SOEC system moves towards a thermoneutral and exothermic mode from endothermic mode at 1 bar. This transition is justified by internal methanation which is favored at higher pressures. Since it is exothermic, more pressure values result in more heat generation inside the SOEC reactor which can offset the heat demand of endothermic electrolysis reactions. However, even at 25 bar, the highest pressure of this study the generated heat inside the SOEC reactor is only 58.6% of the heat absorbed from the TES tanks. This means that at 25 bar the heat generated from the exothermic SOEC reactor still does not amount to the heat consumption from the heat storage tanks. The heat consumed from the TES tanks is not just to meet the heat demand of the SOEC operation but for preheating the inlet gas streams to the SOEC reactor. Thus, even though the heat demand for the SOEC operation is met by exothermic methanation reaction, the TES tanks are vital for the system to keep the boundary conditions . This observation accentuates the results from current density analysis regarding the crucial role of the TES tanks in thermal management of system even at exothermic operation of the SOEC mode. In order to be solely dependent on r-SOC reactor for thermal management of the system α has to be reached to −100%. This is possible at much higher pressure values which on the other hand diminishes the system performance η_{RT_system}

5. Improved system configuration

The parametric analysis on pressure effect demonstrated that higher pressure has positive effect on the r-SOC reactor performance ($\eta_{RT\_reactor}$) while showing a negative effect on the system level performance (η_{RT_system}). The left-y-axis of Fig. 15 shows the variation of

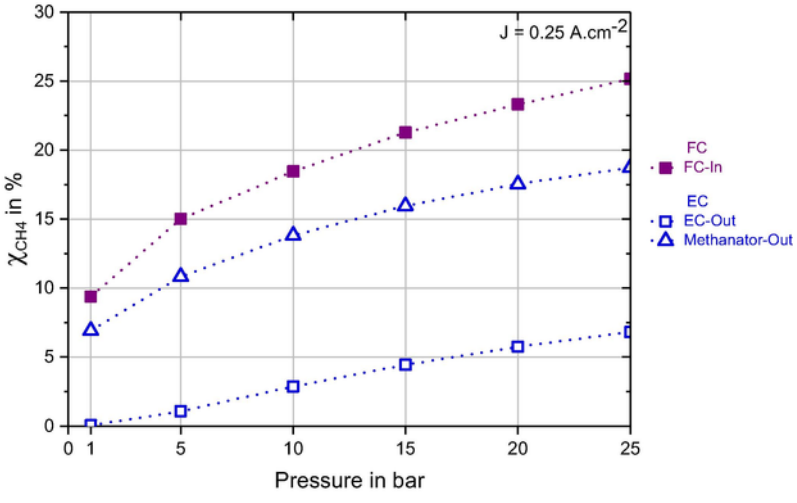

Fig. 13. Effect of pressure on methane composition.

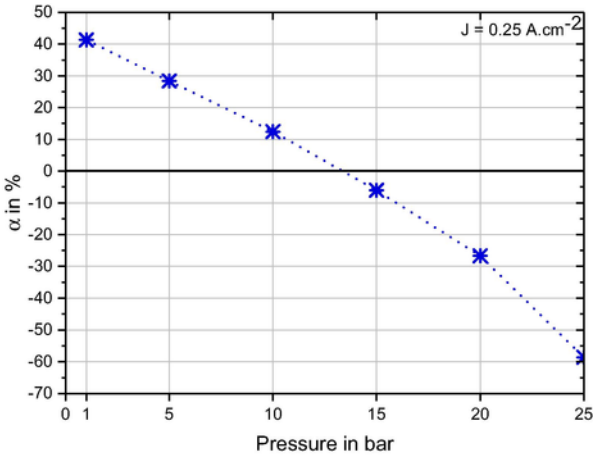

Fig. 14. Effect of pressure on thermal management of SOEC.

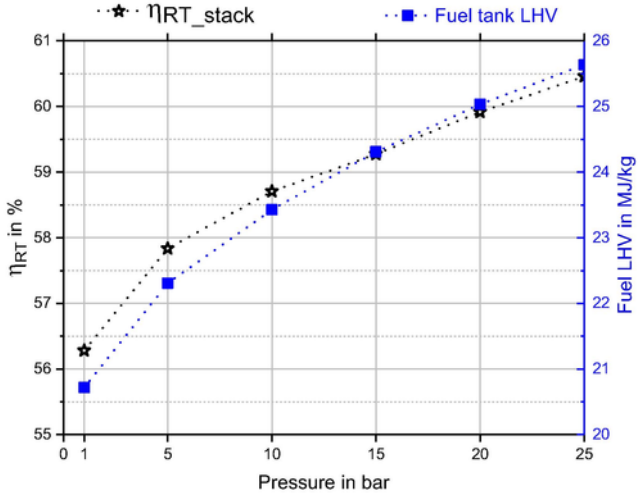

Fig. 15. Effect of pressure on LHV of fuel and reactor round-trip efficiency.

$\eta_{RT\_reactor}$ with p; likewise the right-y-axis of Fig. 15 depicts the effects of p on the LHV content of fuel as an inlet stream to the SOFC reactor. As p increases, the LHV of the fuel injected to the system in SOFC mode rises from 20.7 to 25.6 $MJkg^{-1}$. This enhancement in the LHV is a result of the pressure on the methanation reaction. As mentioned in Section 4.2.2, methanation is favored at higher pressure. LHV of hydrogen, carbon monoxide, and methane are respectively 120, 10, and 50 $MJkg^{-1}$. Due to the growth of methane mass fraction inside the fuel tank at higher pressures and also higher molecular weight of methane, more LHV content is stored in the fuel tank at higher pressures; in other words, less volume of storage tank is required to keep a specific quantity of energy at higher pressures due to higher energy density of methane and other gases. This explains why methanation is important in the r-SOC system both for thermal management and storage tank sizing. As a result of these beneficial impacts of higher pressure on r-SOC reactor performance and fuel quality, an improved system is designed and provided in this paper. The aim of this upgraded system is to make the most of favorable effects of pressure on the r-SOC reactor, which boosts $\eta_{RT\_reactor}$ to 60.5%. Since the unfavorable system performance at higher pressures was mainly caused by the work of the air compressor, the improvement had to be applied on this part of system. Instead of sending the required air from the ambient to the system and compressing it from 1 to 25 bar, it is introduced from a compressed air tank at 25 bar. This solution eliminates the need for high compression ratio of air compressor and thereby lowers the BOP consumption considerably.

5.1. Improved system model and results

The simple schematics of the improved system model are depicted in Figs. 16 and 17 for charging (SOEC) and discharging (SOFC) mode respectively. The system architecture in Aspen Plus® is there-

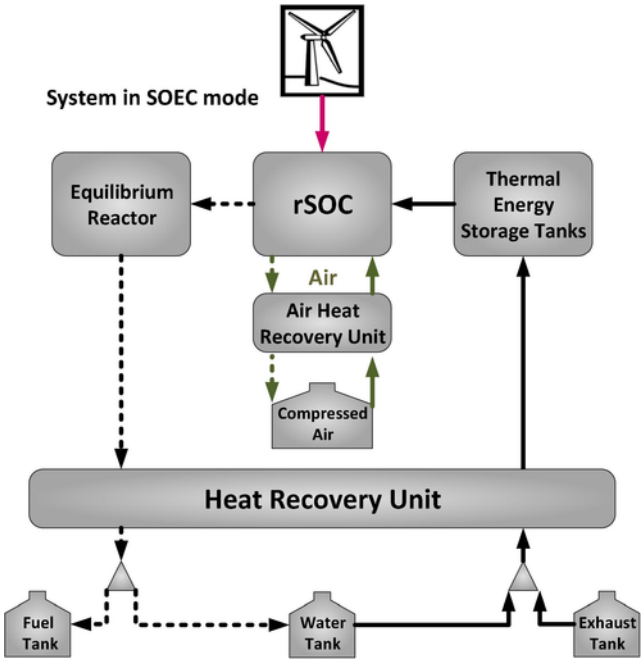

Fig. 16. Simple schematic of improved r-SOC system in charging mode (SOEC).

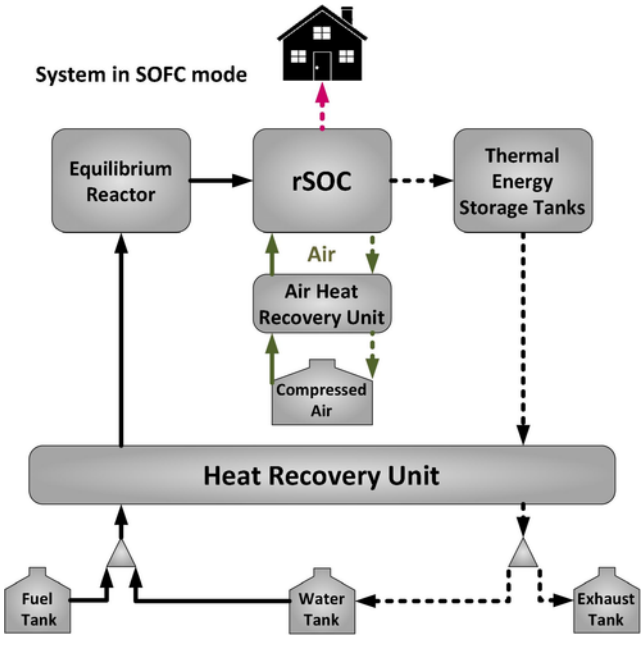

Fig. 17. Simple schematic of improved r-SOC system in charging mode (SOFC).

fore modified accordingly. The results of this improved model along with the system conditions are provided in Table 8.

As shown in the Table 8, the performance of the system has noticeably improved in the upgraded r-SOC system. A remarkable enhancement is observed in η_{RT_system} as the configuration changes from the base model to improved model. In the base model at 25 bar η_{RT_system} dropped to 46% as a result of air compression work. By eliminating the need for air compression in the improved model, η_{RT_system} is boosted to 60.4% (almost by 14%) which is close to $\eta_{RT\_reactor}$. In this improved system design, the parasitic power consumption has largely diminished due to several reasons: (1) The system pressure is at 25 bar which is equal to the gas storage tank pressure. This means that the product gas streams from the system do not need to be compressed from lower system pressures to storage tanks' pressure (25 bar). This equal pressure omits the extra power consumption incurred with the gas compressors. This issue indeed affected the system performance at reference case (p = 1 bar and J = 0.25 $A\ cm^{-2}$) where the round-trip efficiency dropped by 2 points from the reactor to system level ($\eta_{RT\_reactor} = 56.3\%$, $\eta_{RT\_system} = 54.3\%$). (2) The air is not injected from ambient but from a very large compressed air storage tank at 25 bar; hence no compression work is required for the air injection. The assumption of having a large compressed air storage tank is to overcome the oxygen composition change during each half-cycle (charge/discharge) of the system. In other words, having a huge volume of air makes the air composition change due to the electrolysis and oxidation negligible.

Since water is incompressible fluid and is not affected considerably by pressure, it is still kept at 1 bar storage tank and is pumped to system pressure at 25 bar. The power required by pump is not large enough to damage the performance considerably.

As a result of storing all gases at 25 bar in the storage tanks, the parasitic BOP power consumption is avoided and the system performance matches the r-SOC reactor performance. The only issues

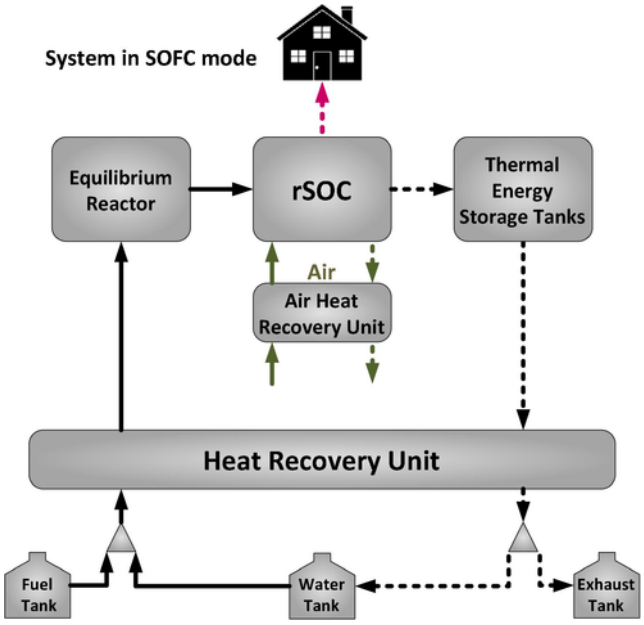

Fig. 2. Simple schematic of r-SOC system in discharging mode (SOFC).

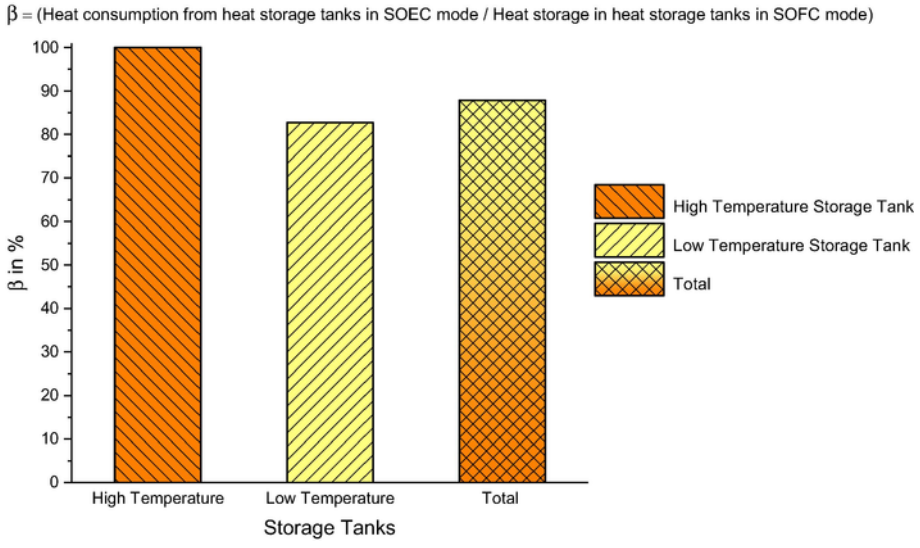

Fig. 6. Ratio of heat consumption from thermal energy storage tanks during SOEC mode.

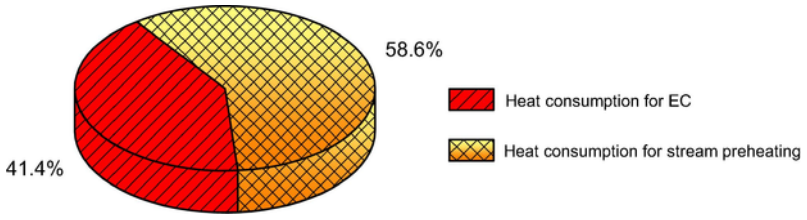

Fig. 7. Comparison of heat required for/released from r-SOC with the heat absorbed from TES tanks in SOEC mode.

Table 8
Conditions and results of improved system model.

Improved system conditions	
p	25 bar
J	0.25 A cm^{-2}
U_{SOFC}	85%
Improved system results in %	
$\eta_{RT\_reactor}$	60.5
η_{RT_system}	60.4
U_{SOEC}	65
α	−58.6

Table 9
Abbreviation, nomenclature, and sign convention table.

Abbreviation	Description
ASC	Anode Supported Cell
ASR	Area Specific Resistance
BOP	Balance Of Plant
DLR	Deutsches Zentrum für Luft- und Raumfahrt
EES	Electrical Energy Storage
ESC	Electrolyte Supported Cell
GDC	Galodenium doped Ceria
H/C ratio	Hydrogen to Carbon ratio
HTF	Heat Transfer Fluid
HT-ST	High Temperature Storage Tank
LHS	Latent Heat Storage
LHTES	Latent Heat Thermal Energy Storage
LSCF	Lanthanum Strontium Cobalt Ferrate
LSM	Lanthanum Strontium Manganite
LT-ST	Low Temperature Storage Tank
O/C ratio	Oxygen to Carbon ratio
PCM	Phase Change Material
PFD	Process Flow Diagram
RES	Renewable Energy Sources
r-SOC	Reversible Solid Oxide Cell
RWGS	Reverse Water Gas Shift
S/C ratio	Steam to Carbon ratio
SHS	Sensible Heat Storage
SMR	Steam Methane Reforming
SOC	Solid Oxide Cell
SOEC	Solid Oxide Electrolysis Cell
SOFC	Solid Oxide Fuel Cell
TES	Thermal Energy Storage
WGS	Water Gas Shift
YSZ	Yttria Stabilized Zirconia
Aspen plus components	
RGibbs	Equilibrium reactor with Gibbs energy Minimization
RStoic	Stoichiometric reactor with specified reaction extent or conversion
REquil	Equilibrium reactor with chemical and phase equilibrium reactions
Nomenclature	
Chemical formulas	
CH_4	methane
CO	carbon monoxide
CO_2	carbon dioxide
H_2	hydrogen
H_2O	water
KF	potassium fluoride
LiF	lithium fluoride
MgF_2	magnesium fluoride
N_2	nitrogen
Ni	nickel
O_2	oxygen
Roman letters	
ASR	area specific resistance, Ωcm^2
C_p	specific heat capacity at constant pressure, $J\,kg^{-1}K^{-1}$

Table 9 (*Continued*)

Abbreviation	Description
F	Faraday constant, $\mathrm{C\ mol^{-1}}$
H	specific enthalpy, $\mathrm{J\ kg^{-1}}$
I	current, A ($\mathrm{Cs^{-1}}$)
J	current density, $\mathrm{A\ cm^{-2}}$
$\dot{m}$	mass flow rate, $\mathrm{kg\ s^{-1}}$
$\dot{n}$	molar flow rate, $\mathrm{mol\ s^{-1}}$
p	pressure, bar
p_i	partial pressure of component i, bar
P_{r-SOC}	power consumption or generation by r-SOC reactor, W
P_{SOFC}	power generation by SOFC, W
P_{SOEC}	power consumption by SOEC, W
q	electric charge, C
Q	heat, W
Q_{Cons}	total heat consumed from both heat storage tanks in SOEC mode, W
$Q_{process}$	heat remained in process streams after passing heat storage tanks, W
Q_{SOFC}	heat generation by SOFC, W
Q_{SOEC}	heat consumption/generation by SOEC, W
$Q_{storage}$	total heat stored in both heat storage tanks in SOFC mode, W
$U_{f,SOC}$	utilization factor of reactants in SOC reactor, %
$U_{f,SOFC}$	percentage of inlet gases that are utilized in reactions of SOFC reactor, %
$U_{f,SOEC}$	percentage of inlet gases that are utilized in reactions of SOEC reactor, %
R	universal gas constant, $\mathrm{J\ mol^{-1}K^{-1}}$
$Relative P_{BOP,SOFC}$	normalized $\sum P_{BOP,SOFC}$ with respect to P_{SOFC}, %
$Relative P_{BOP,SOEC}$	normalized $\sum P_{BOP,SOEC}$ with respect to P_{SOEC}, %
T	time, s
T	temperature, K
T_l	temperature of material in liquid state, K

Table 9 (*Continued*)

Abbreviation	Description
T_m	melting temperature of material, K
T_s	temperature of material in solid state, K
$\bar{z}$	number of exchanged electrons during electrochemical reactions, –
V_{cell}	operating voltage of single cell in r-SOC reactor, V
V_{loss}	overpotential losses (electrochemical losses), V
V_{Nernst}	ideal voltage of r-SOC reactor without electrochemical losses (Outlet Nernst voltage), V
V_{TN}	thermoneutral voltage, V
Greek letters	
α	ratio of Q_{SOEC} to Q_{Cons} in SOEC mode, %
ΔG°	standard Gibbs free energy of formation, $J\ mol^{-1}$
Δh	specific enthalpy change of reaction, $J\ mol^{-1}$
$\Delta \dot{H}_{rxn,SOC}$	total enthalpy change of reactions inside SOC either in SOFC or SOEC mode, W
ΔT	temperature difference between inlet/outlet of SOC reactor, K
η_{RT}	Round-Trip Efficiency, %
$\eta_{RT\_reactor}$	r-SOC reactor efficiency as a ratio of P_{SOFC} to P_{SOEC}, %
$\eta_{RT_{system}}$	system efficiency as a function of r-SOC reactor performance and BOP, %
$\sum P_{BOP,SOFC}$	net power of system associated with BOP components in SOFC, W
$\sum P_{BOP,SOEC}$	net power of system associated with BOP components in SOEC, W
χ_i	molar composition of component i, %
Subscripts	
charging	electrolysis/reduction
chemical	chemical power remained in streams at the end of SOFC operation
Com	compressor
Cons	consumption
discharging	fuel cell/ oxidation
exp	expander

Table 9 (*Continued*)

Abbreviation	Description
f	final
i	initial
in	inlet
l	liquid
m	melting point
out	outlet
pg	Process Gas
rxn	reaction
s	solid
TN	thermoneutral
TOT	total heat stored in/consumed from heat storage tanks
Sign convention	
Heat/electricity consumption	+
Heat/electricity generation	−

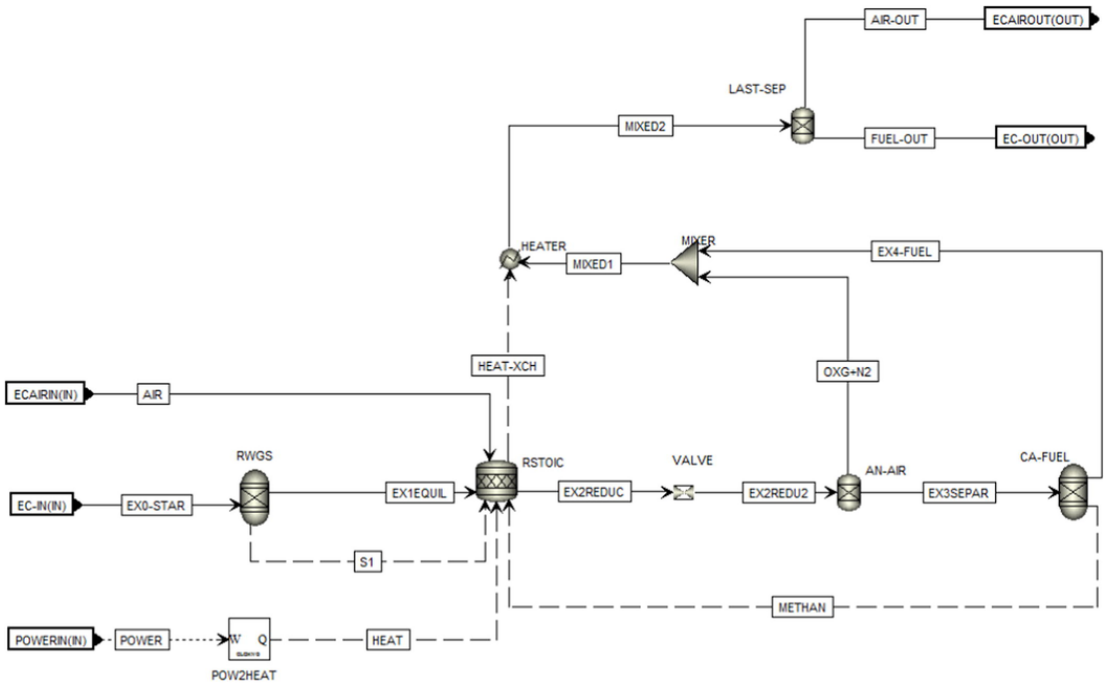

Fig. A.1. SOEC model in AspenPlus.

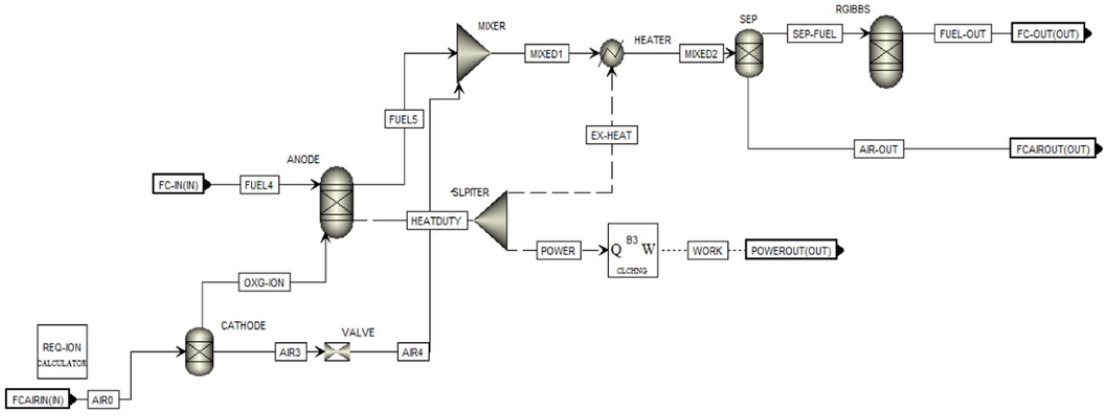

Fig. A.2. SOFC model in AspenPlus.

diminishing the performance are pressure drop, friction, and work performed by the pump .

Therefore, the best practical working condition for the designed r-SOC system is at p = 25 bar, J = 0.25 $A\ cm^{-2}$ and storage tank conditions of p = 25 bar and T = 110 °C for the process gases and p = 25 bar and T = 25 °C for the air.

6. Conclusion

An energy storage system is designed based on a reversible solid oxide cell (r-SOC) reactor which is commercially available . The parametric analysis reveals the following results on the r-SOC behavior and performance:

- At reference conditions, p = 1 bar and J = 0.25 $A\ cm^{-2}$, round-trip efficiency of the r-SOC reactor reaches to $\eta_{RT\_reactor} = 56.3\%$; however, due to the parasitic BOP consumption the round-trip efficiency of system is lower $\eta_{RT\_system} = 54.3\%$.
- A full thermally self-sustaining r-SOC system is achieved by storing generated heat during the SOFC mode and utilizing it during the SOEC mode.
- Using phase change materials with proper melting point in latent heat storage tanks facilitates the thermal management of system and eliminates the need for external heat sources.
- Presence of thermal energy storage system is vital for the system as it not only provides heat for endothermic operation of the SOEC, but also heats up the inlet streams of the SOEC to the boundary condition temperature.
- The significance of latent heat storage system has been realized particularly after parametric analysis. In spite of the fact that the electrolyzer enters its exothermic mode, the amount of heat released from the SOEC was not sufficient to meet the heat demand for preheating the inlet streams.
- Q_{SOEC} released from exothermic operation of the SOEC reactor at highest value of current density (J = 0.45 $A\ cm^{-2}$) and pressure

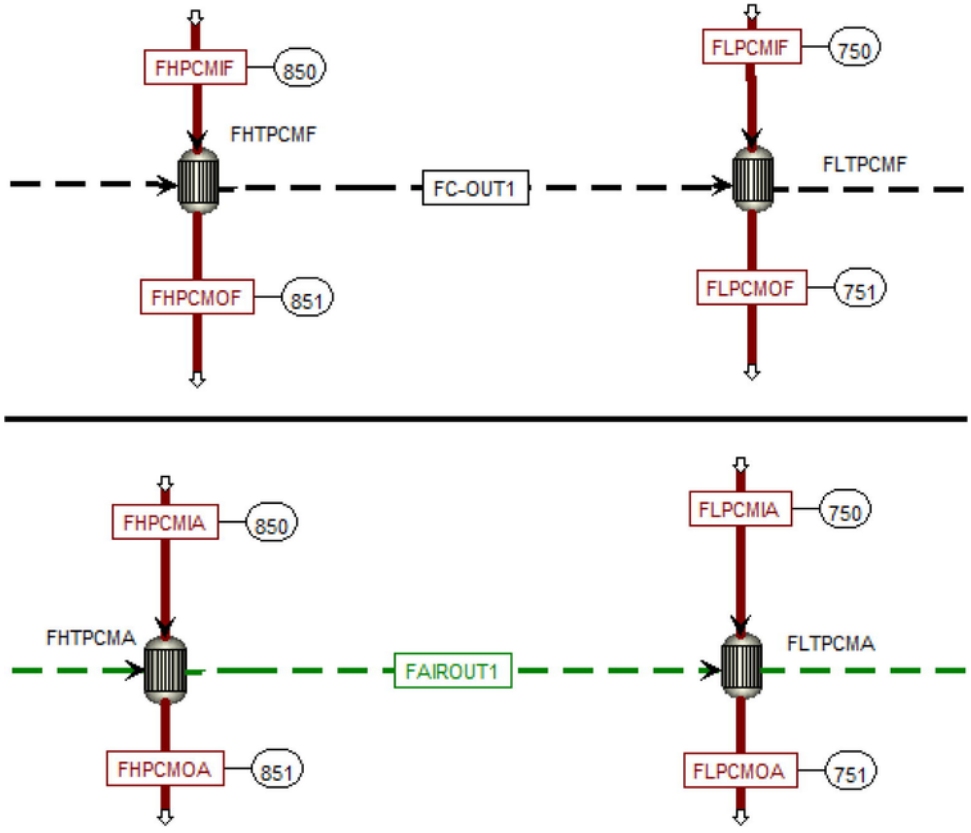

Fig. B.1. Latent heat storage system model in AspenPlus.

(p = 25 bar) is only 34.8% and 58.6% of the total heat demand of the process streams, respectively.

- Increase of pressure positively affects $\eta_{RT\_reactor}$ while negatively affects η_{RT_system}. At p = 25 bar, $\eta_{RT\_reactor}$ reaches 60.5% whereas η_{RT_system} drops to 46%. This mismatch in the pressure effect is due to parasitic BOP consumption caused by higher compression ratios of air compressors at higher pressures.
- To abate the high and detrimental BOP consumptions at higher pressures, an improved system model is designed. The system pressure in this upgraded model is 25 bar in order to make the most of a good r-SOC reactor performance at this pressure.
- In the improved model, the air is supplied from a pressurized storage tank at 25 bar (compressed air tank) instead of air at ambient conditions. This solution eliminates most of the BOP consumption as there is no considerable compression work for air. Moreover, at a system pressure of 25 bar, no compression work is required to compress outlet process gases from the system to the gas storage tank (25 bar).
- As a result of this enhanced system configuration, η_{RT_system} reaches 60.4% which is very close to $\eta_{RT\_reactor}$ at 25 bar, 60.5%. The difference is a result of pressure drops in the pipelines and valves.
- In comparison with reference case (p = 1 bar, J = 0.25 $A\ cm^{-2}$, air supply from ambient), the improved model (p = 25 bar, J = 0.25 $A\ cm^{-2}$, air supply from compressed storage tank) has remarkably better performance in terms of the r-SOC reactor and system round-trip efficiency.
- The system behavior is dependent on design and performance of the r-SOC reactor, the better the reactor $\eta_{RT_{reactor}}$ the better the reactor $\eta_{RT_{system}}$.

Acknowledgements

The author would like to thank Dr. Moritz Henke for his scientific discussion about the improved system analysis and would like to thank Dr. Seyed Schwan Hosseiny for the language corrections..

Appendix A

Implementation of r-SOC reactor for both SOFC and SOEC mode in Aspen Plus (see Figs. A.1 and A.2).

Implementation of latent heat storage system for both high and low temperature storage tanks (see Fig. B.1).

References

[1] X. Luo, J. Wang, M. Dooner, J. Clarke, Overview of current development in electrical energy storage technologies and the application potential in power system operation, Appl Energy 137 (2015) 511–536.

[2] E. Yao, H. Wang, L. Wang, G. Xi, F. Maréchal, Multi-objective optimization and exergoeconomic analysis of a combined cooling, heating and power based compressed air energy storage system, Energy Convers Manag 138 (2017) 199–209.

[3] P.K. Shen, C.-Y. Wang, S.P. Jiang, X. Sun, J. Zhang, Electrochemical energy: advanced materials and technologies, 1st ed., CRC Press, 2016.

[4] S. Lv, W. He, A. Zhang, G. Li, B. Luo, X. Liu, Modelling and analysis of a novel compressed air energy storage system for trigeneration based on electrical energy peak load shifting, Energy Convers Manag 135 (2017) 394–401.

[5] A. Mohammadi, M.H. Ahmadi, M. Bidi, F. Joda, A. Valero, S. Uson, Exergy analysis of a Combined Cooling, Heating and Power system integrated with wind turbine and compressed air energy storage system, Energy Convers Manag 131 (2017) 69–78.

[6] H. Jou, Y. Chang, J. Wu, K. Wu, Operation strategy for a lab-scale grid-connected photovoltaic generation system integrated with battery energy storage, Energy Convers Manag 89 (2015) 197–204.

[7] N.C. Nair, N. Garimella, Battery energy storage systems: assessment for small-scale renewable energy integration, Energy Build 42 (11) (2010) 2124–2130.

[8] C.H. Wendel, P. Kazempoor, R.J. Braun, Novel electrical energy storage system based on reversible solid oxide cells: system design and operating conditions, J Power Sources 276 (2015) 133–144.

[9] O.J. Shariatzadeh, A.H. Refahi, S.S. Abolhassani, M. Rahmani, Modeling and optimization of a novel solar chimney cogeneration power plant combined with solid oxide electrolysis/fuel cell, Energy Convers Manag 105 (2015) 423–432.

[10] Alcaide F, Brillas E. Fuel cells for chemicals and energy cogeneration. 2006; 153: 47–60.

[11] K. Xie, Y. Zhang, G. Meng, J.T.S. Irvine, Direct synthesis of methane from CO_2/H_2O in an oxygen-ion conducting solid oxide electrolyser, Energy Environ Sci 4 (2011) 2218–2222.

[12] P. Kazempoor, R.J. Braun, Model validation and performance analysis of regenerative solid oxide cells: electrolytic operation, Int J Hydrogen Energy 39 (6) (2014) 2669–2684.

[13] Monti A, Wendel CH, Santarelli M, Braun RJ. Energy dense storage using intermediate temperature reversible solid oxide cell systems. 2015; 68(1): 3289–300.

[14] C.H. Wendel, P. Kazempoor, R.J. Braun, A thermodynamic approach for selecting operating conditions in the design of reversible solid oxide cell energy systems, J Power Sources 301 (2016) 93–104.

[15] D. Ferrero, A. Lanzini, P. Leone, M. Santarelli, Reversible operation of solid oxide cells under electrolysis and fuel cell modes: experimental study and model validation, Chem Eng J 274 (2015) 143–155.

[16] Di Giorgio P, Desideri U. Potential of reversible solid oxide cells as electricity storage system; 2016.

[17] H. Fan, M. Keane, P. Singh, M. Han, Electrochemical performance and stability of lanthanum strontium cobalt ferrite oxygen electrode with gadolinia doped ceria barrier layer for reversible solid oxide fuel cell, J Power Sources 268 (2014) 634–639.

[18] Y. Rao, Z. Wang, W. Zhong, R. Peng, Y. Lu, Novel Ni-$Ba_{1+x}Zr_{0.3}Ce_{0.5}Y_{0.2}O_{3-\delta}$ hydrogen electrodes as effective reduction barriers for reversible solid oxide cells based on doped ceria electrolyte thin film, J Power Sources 199 (2012) 142–145.

[19] M. Choi, B. Singh, E.D. Wachsman, S. Song, Performance of $La_{0.1}Sr_{0.9}Co_{0.8}Fe_{0.2}O_{3-\delta}$ and $La_{0.1}Sr_{0.9}Co_{0.8}Fe_{0.2}O_{3-\delta}$–$Ce_{0.9}Gd_{0.1}O_2$ oxygen electrodes with $Ce_{0.9}Gd_{0.1}O_2$ barrier layer in reversible solid oxide fuel cells, J Power Sources 239 (2013) 361–373.

[20] P. Costamagna, A. Selimovic, M. Del Borghi, G. Agnew, Electrochemical model of the integrated planar solid oxide fuel cell (IP-SOFC), Chem Eng J 102 (1) (2004) 61–69.

[21] N.Q. Minh, M.B. Mogensen, Reversible solid oxide fuel cell technology for green fuel and power production, Electrochem Soc Interface 22 (4) (2013) 55–62.

[22] D.M. Bierschenk, J.R. Wilson, S.A. Barnett, High efficiency electrical energy storage using a methane – oxygen solid oxide cell, Energy Environ Sci (2011) 944–951.

[23] S.H. Jensen, C. Graves, M. Mogensen, C. Wendel, R. Braun, G. Hughes, et al., Environmental Science Large-scale electricity storage utilizing reversible solid oxide cells combined with underground, Energy Environ Sci 8 (2015) 2471–2479.

[24] C.H. Wendel, Z. Gao, S.A. Barnett, R.J. Braun, Modeling and experimental performance of an intermediate temperature reversible solid oxide cell for high-efficiency, distributed-scale electrical energy storage, J Power Sources 283 (2015) 329–342.

[25] Xu HJ, Zhao CY. Thermodynamic analysis and optimization of cascaded latent heat storage system for energy efficient utilization 2015; 90: 1662–73.

[26] C. Willich, C. Westner, M. Henke, F. Leucht, J. Kallo, K.a. Friedrich, Pressurized solid oxide fuel cells with reformate as fuel, J Electrochem Soc 159 (11) (2012) F711–F716.

[27] Steele BCH, Heinzel A. Materials for fuel-cell technologies 2001; 414: 345–52.

[28] Ding C, Hashida T. High performance anode-supported solid oxide fuel cell based on thin-film electrolyte and nanostructured cathode. 2010; 95: 1729–31.

[29] Su S, Gao X, Zhang Q, Kong W, Chen D. Anode- versus cathode-supported solid oxide fuel cell : effect of cell design on the stack performance 2015; 10: 2487–503.

[30] Kim J, Song R, Song K, Hyun S, Shin D, Yokokawa H. Fabrication and characteristics of anode-supported flat-tube solid oxide fuel cell 2003; 122: 138–43.

[31] X. Lv, C. Lu, Y. Wang, Y. Weng, Effect of operating parameters on a hybrid system of intermediate- temperature solid oxide fuel cell and gas turbine, Energy 91 (2015) 10–19.

[32] Singhal SC, Kendall K. High-temperature solid oxide fuel cells: fundamentals, design and applications 2003; 7(1).

[33] M. Mogensen, F. Allebrod, J.R. Bowen, C. Chatzichristodoulou, M. Chen, S.D. Ebbesen, et al., Electrolysis for integration of renewable electricity and routes towards sustainable fuels, In: 10th International workshop on large-scale integration of wind power into power systems as well as on transmission networks for offshore wind farms, 2011.

[34] Porubova J, Klemm M, Kiendl I, Valters K, Markova D, Repele M. Influence of temperature and pressure change on adiabatic and isothermal methanation processes 2012: 22–27.

[35] J. Pawel, O. Lian, Q. Sun, S. Hwa, Energy and exergy analysis of Solid Oxide Electrolyser Cell (SOEC) working as a CO_2 mitigation device, HE 37 (19) (2012) 14518–14527.

[36] Ni M, Leung MKH, Leung DYC. Technological development of hydrogen production by solid oxide electrolyzer cell (SOEC). 2008; 33: 2337–54.

[37] Moyer CJ, Ambrosini A, Sullivan NP, Kee RJ, Stechel EB. Solid oxide electrochemical reactor science; 2010.

[38] Sharma A, Tyagi VV, Chen CR, Buddhi D. Review on thermal energy storage with phase change materials and applications. 2009; 13: 318–45.

[39] S. Kuravi, J. Trahan, D.Y. Goswami, M.M. Rahman, E.K. Stefanakos, Thermal energy storage technologies and systems for concentrating solar power plants, Prog Energy Combust Sci 39 (4) (2013) 285–319.

[40] S. Motahar, A.A. Alemrajabi, R. Khodabandeh, Experimental study on solidification process of a phase change material containing TiO_2 nanoparticles for thermal energy storage, Energy Convers Manag 138 (2017) 162–170.

[41] Zalba B, Marin JM, Cabeza LF, Mehling H. Review on thermal energy storage with phase change: materials, heat transfer analysis and applications, 2003; 23.

[42] A. Kumar, S.K. Shukla, A review on thermal energy storage unit for solar thermal power plant application, Energy Procedia 74 (2015) 462–469.

[43] K. Großmann, P. Treiber, J. Karl, Steam methane reforming at low S/C ratios for power-to-gas applications, Int J Hydrogen Energy 1 (2016) 1–9.

[44] Barelli LÃ, Bidini G, Gallorini F, Servili S. Hydrogen production through sorption-enhanced steam methane reforming and membrane technology: a review. 2008; 33: 554–70.

[45] Y. Wang, F. Yoshiba, M. Kawase, T. Watanabe, Performance and effective kinetic models of methane steam reforming over Ni/YSZ anode of planar SOFC, Int J Hydrogen Energy 34 (9) (2009) 3885–3893.

[46] D.A. Saletore, W.J. Thomson, Methanation reaction rates for recycle reactor compositions, Ind Eng Chem Process Des Dev 16 (1) (1977) 70–75.

[47] Gao J, Wang Y, Ping Y, Hu D, Xu G, Su F. RSC Advances PAPER A thermodynamic analysis of methanation reactions of carbon oxides for the production of synthetic natural gas. 2012: 2358–68.

[48] De Groot A. Advanced exergy analysis of high temperature fuel cell systems, TU Delft; 2004.

[49] Heddrich MP, Jahn M, Michaelis A, Näke R, Weder A. SOFC system design using ideal efficiency modeling – model and experimental implementation 2013; 4: 612–22.

[50] Dunbar WR. Emf 5 maximum power and efficiency of fuel cells 2016; 115(June 1993): 5–9.

[51] A.V. Virkar, Transport through mixed proton, oxygen ion and electron/hole conductors: analysis of fuel cells and electrolyzer cells using Onsager equations, Int J Hydrogen Energy 37 (17) (2012) 12609–12628.

[52] Riedel M, Heddrich MP, Friedrich KA. Pressurized operation of a 10 layer solid oxide electrolysis stack. 2016; 911(July): 97–101.

[53] Misra AK, Whittenberger JD. Fluoride salts and container materials for thermal energy storage applications in the temperature range 973 to 1400 K; 1987.

[54] M.M. Kenisarin, High-temperature phase change materials for thermal energy storage, Renew Sustain Energy Rev 14 (3) (2010) 955–970.

[55] S. Santhanam, C. Schilt, B. Turker, T. Woudstra, P.V. Aravind, Thermodynamic modeling and evaluation of high efficiency heat pipe integrated biomass Gasifier–Solid Oxide Fuel Cells–Gas Turbine systems, Energy 109 (2016) 751–764.

[56] Sehested J, Dahl S, Jacobsen J, Rostrup-nielsen JR. Methanation of CO over nickel: mechanism and kinetics at high H_2/CO ratios. 2005: 2432–8.

[57] D. Hu, J. Gao, Y. Ping, L. Jia, P. Gunawan, Z. Zhong, et al., Enhanced investigation of CO methanation over Ni/Al_2O_3 catalysts for synthetic natural gas production, Ind Eng Chem Res 51 (13) (2012) 4875–4886.